Journal of AppliedMath 2023; 1(2): 237.
Original Research Article

Enhanced medicinal applications of Co-doped $Zn_{0.5}Ni_{0.5}Fe_{2-x}O_4$ for (X = 0.00 and 0.0250) soft ferrites: A structural analysis

Abu Zar Muaawia[1], Ali Mujtaba[2,*], M. I. Khan[2], Babar Ali[3], Ansa Karamat[4], Adnan Asghar[5]

[1] *Department of Physics, University of the Punjab, Lahore 54590, Punjab, Pakistan*

[2] *Department of Physics, The University of Lahore, Lahore 53700, Punjab, Pakistan*

[3] *Department of Physics, University of Okara, Okara 56300, Punjab, Pakistan*

[4] *Department of Physics, GC Women University Sialkot, Punjab 51310, Pakistan*

[5] *School of Quantitative Sciences, UUM College of Arts & Sciences, Universiti Utara Malaysia, UUM Sintok 06010, Kedah Darul Aman, Malaysia*

*** Corresponding author:** Ali Mujtaba, alimujtabaaslam@gmail.com

ARTICLE INFO

Received: 18 June 2023
Accepted: 26 July 2023
Available online: 5 August 2023

doi: 10.59400/jam.v1i2.237

ABSTRACT: In this experimental research paper, we investigate the potential enhancement of Co-doped $Zn_{0.5}Ni_{0.5}Fe_{2-x}Co_xO_4$ for (x = 0.0, and 0.0250) ferrites synthesized by the green synthesis method for applications in medicine. The structural analysis of the synthesized material is a crucial step in understanding its suitability for medical applications. X-ray diffraction (XRD) is employed to elucidate the crystallographic structure of the Co-doped $ZnNiFe_2O_4$ ferrites. The results demonstrate that the doping process has a significant influence on the material's crystal structure, which may impact its potential in various biomedical applications. The Co-doped $ZnNiFe_2O_4$ spinel ferrite materials become more suitable for medical applications as the decrease in X-ray density and simultaneous increase in bulk density can facilitate better tissue penetration and biocompatibility, making them ideal for non-invasive medical imaging and therapeutic applications, while minimizing potential health risks.

KEYWORDS: ferrites application; medicine; XRD; spinel ferrites; Co-doping

1. Introduction

$ZnNiFe_2O_4$ ferrites have garnered interest in recent years for their potential applications in the field of medicine, including drug delivery systems, magnetic resonance imaging (MRI) contrast agents, and hyperthermia therapy. One such area of research is the co-doping of materials, where multiple dopants are introduced into a host material to modify its properties. Doping these ferrites with transition metals like cobalt (Co) can potentially enhance their magnetic and structural properties, making them even more suitable for medical applications[1,2].

The structural analysis of co-doped $ZnNiFe_2O_4$ is crucial to understanding the changes in its crystal structure, lattice parameters, and bonding characteristics. Li et al.[3] investigated the structural and magnetic properties of Co-doped $BiLaFeCoO_3$ nanoparticles using XRD. The results showed that Co-doping on the A sites decreased the lattice parameters and increased the magnetic permeability[4–6]. Ameen et al.[7] used XRD to study the structural and morphological properties of Mg-doped $ZnNiFe_2O_4$ nanoparticles. The results showed that Mg-doping on the A sites resulted in an increase in coercive and saturation magnetization. They investigated the thermal stability and magnetic properties of Mg-doped

$ZnNiFe_2O_4$ nanoparticles. The results showed that Mg-doping on the A sites increased the thermal stability of the nanoparticles and improved their magnetic properties[7]. Wu et al.[8] used XRD to study the structural and morphological properties of Co-doped $ZnMgFe_2O_4$ nanoparticles for drug delivery[9,10]. The results showed that Co-doping on the A sites improved the dispersion and loading capacity of the nanoparticles for drug delivery. Mujtaba et al.[11] tailored the structural, optical, electrical, and photoluminescence properties of $ZnNiMgFe_{2-x}La_xO_4$, which showed better crystal structure and improvement in optical properties[12–15].

The structural, optical, electrical, and dielectric properties of soft ferrites are significantly influenced by the technique of manufacture and sintering temperature. Various techniques can be employed for the fabrication of nanomaterials, including sol-gel, hydrothermal, combustion, co-precipitation, and green synthesis approaches[16,17]. The implementation of green synthesis techniques has the potential to mitigate the environmental consequences associated with chemical synthesis, mostly due to their reduced utilization of hazardous chemicals and diminished waste generation. Ginger has been employed in the process of green synthesis for a multitude of applications[18–20]. As an illustration, it has been employed as an inherent catalyst to synthesize various chemicals, including gold nanoparticles and silver nanoparticles. The antioxidant capabilities and metal ion oxidation reduction efficacy of ginger's active components, including gingerol and shogaol, have been documented in scientific research. Hence, the utilization of ginger extract (19 g/100 mL) as a potential reducing agent in the synthesis of spinel ferrites has been proposed[20,21].

In conclusion, the co-doping of materials has emerged as a promising strategy to enhance their properties for various applications. In this study, we focus on the synthesis and structural characterization of Co-doped $Zn_{0.5}Ni_{0.5}Fe_{2-x}Co_xO_4$ ferrites (x = 0.0 and 0.0250) using XRD to assess their suitability for medical applications. The green synthesis method is used to synthesize $Zn_{0.5}Ni_{0.5}Fe_{2-x}Co_xO_4$. The structural properties of co-doped $Zn_{0.5}Ni_{0.5}Fe_{2-x}Co_xO_4$ will be investigated using techniques such as XRD. The enhanced properties of co-doped $Zn_{0.5}Ni_{0.5}Fe_{2-x}Co_xO_4$, including electrical, magnetic, and catalytic properties, will be evaluated for potential medicinal applications. The findings of this study will contribute to the understanding of co-doped materials and their potential in the field of medicine.

2. Materials and methods

The pure and doped $Zn_{0.5}Ni_{0.5}Fe_{2-x}Co_xO_4$ samples with x values of 0.0 and 0.0250 were synthesized using the green synthesis method. Initially, a solution was made by combining 250 mL of distilled water and 48 g of ginger. This mixture was subjected to 15 min of boiling with magnetic agitation, resulting in the formation of a brown-colored solution. The sample was allowed to settle to ambient temperature before being filtered. In addition, a solution of 12 g of sodium hydroxide (NaOH) dissolved in 100 mL of distilled water was produced by magnetic agitation for one hour. Additionally, nickel nitrate $Ni(NO_3)_2.6H_2O$, cobalt nitrate $Co(NO_3)_2.6H_2O$, zinc nitrate $Zn(NO_3)_2.6H_2O$, and ferric nitrate $Fe(NO_3)_2.9H_2O$ were solubilized in a 200-mL ginger solution containing 48 g of ginger. The solution was subsequently stirred magnetically and heated at 80 ℃ for one hour on a hot plate. Subsequently, a NaOH solution was added gradually to the mixture while maintaining constant agitation until the pH of the resulting solution reached 12. To obtain the final product, the solution was centrifuged. To facilitate further characterization, the collected samples were subjected to a dehydrating procedure and then finely pulverized. Using the same procedure, $Zn_{0.5}Ni_{0.5}Fe_{2-x}Co_xO_4$ was synthesized using a 250 mL ginger solution. The block diagram representing the methodology is depicted in **Figure 1**.

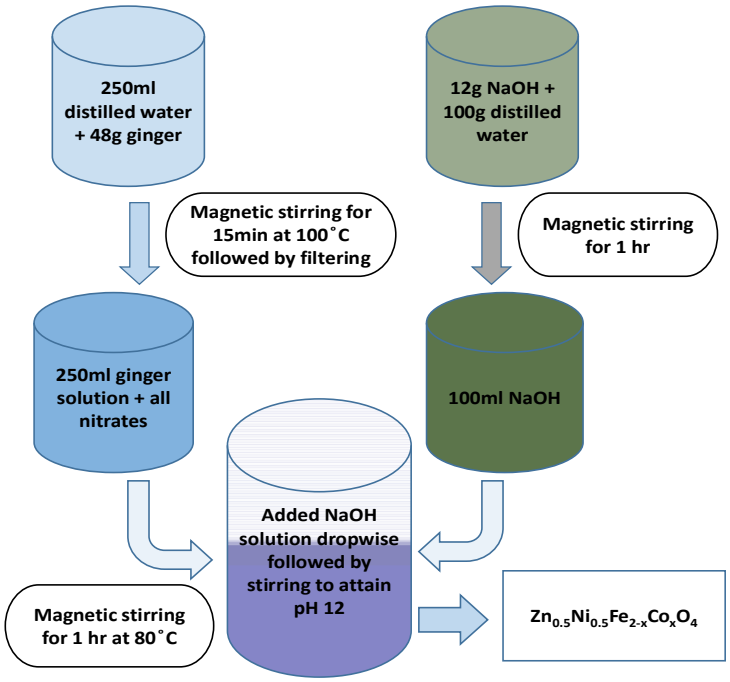

Figure 1. Block diagram of experimental methodology for Co doped soft ferrites.

3. Results and discussions

Structural properties

Figure 2 displays the X-ray diffraction (XRD) patterns of $Zn_{0.5}Ni_{0.5}Fe_{2-x}Co_xO_4$ samples, namely those with x values of 0.00 and 0.025. These soft ferrite samples were synthesized using the co-precipitation method. The X-ray diffraction (XRD) analysis indicated the successful incorporation of Co^{3+} ions into the $Zn_{0.5}Ni_{0.5}Fe_{2-x}Co_xO_4$ ferrite structure. The introduction of Co intensity at a doping concentration of x = 0.0250 results in the generation of the highest peak (311)[11].

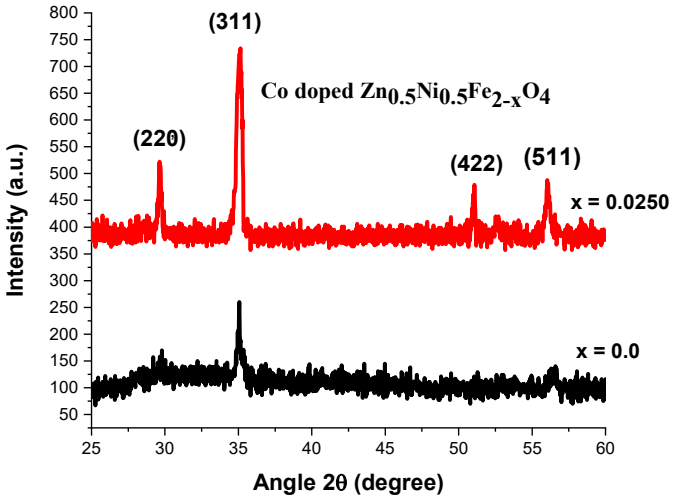

Figure 2. XRD patterns of $Zn_{0.5}Ni_{0.5}Fe_{2-x}Co_xO_4$ for x = 0.00, and 0.0250.

The subsequent equation was employed to get the mean crystallite size[2]:

$$D = \frac{0.9\lambda}{\beta cos\theta} \quad (1)$$

The symbol β represents the full width at half maximum (FWHM) of the X-ray diffraction (XRD) peaks, while the wavelength is denoted by λ = 1.542 Å. **Table 1** displays the observed variations in numerical values of different structural characteristics of $Zn_{0.5}Ni_{0.5}Fe_{2-x}Co_xO_4$ ferrites as determined through X-ray diffraction (XRD) analysis. In the case of the sample with x = 0.00, the largest observed crystallite size was measured to be 72.8 nm. However, for the sample with x = 0.0250, the crystallite size was reduced to 18.2 nm. The difference in ionic radii can be explained by the variation in the values of Co^{3+} (0.58 Å) and Fe^{3+} (0.63 Å)[11]. The equation provided is utilized for the computation of lattice parameters, and the resultant values are presented in **Table 1**:

$$a_{\text{exp}} = d\sqrt{h^2 + k^2 + l^2} \quad (2)$$

The *d*-spacing and Miller indices, denoted as *d, h, k* and *l*, respectively, are fundamental concepts in crystallography. The *d*-spacing represents the distance between adjacent crystal lattice planes, while the Miller indices describe the orientation and location of these planes within the crystal structure[7]. The calculation of d-spacing involves the application of Bragg's equation, which relates the angle of incidence of X-rays or other electromagnetic waves to the spacing between crystal lattice planes[22]:

$$d = \frac{n\lambda}{2sin\theta} \quad (3)$$

The variables n and θ represent the diffraction order and the angle of diffraction, respectively. The lattice constant exhibited a drop from an initial value of 8.493 Å to a final value of 8.470 Å. **Figure 3** illustrates the variation in lattice constant among all nanoferrites. The observed changes in lattice constant for Co^{3+}-doped soft ferrites can be attributed to the difference in ionic radii between Co^{3+} (0.58 Å) and Fe^{3+} (0.63 Å). The increase in the concentration of Co^{3+} ions, which possess smaller ionic radii, leads to the replacement of Fe^{3+} ions with larger radii[23]. The aforementioned result was derived by Mostafa et al. According to Vegard's principle, when the ionic radius of replacing ions is smaller than that of host ions, there is a decrease in the lattice constant. In contrast, the peak with the highest degree of sharpness (311), tends to shift towards larger angles with the introduction of Co^{3+} concentrations[24]. The displacement seen can be attributed to the difference in ionic radii between cobalt (Co) and iron (Fe). Hasan et al. observed a similar phenomenon of displacement. The introduction of Co concentration leads to an increase in intensity at peaks (422) and (511), confirming the presence of doping material and the creation of a cubic structure. The density of X-ray (d_x), bulk density (d_b), and porosity were determined using the following relationships[25]:

$$d_x = \frac{Zm}{\text{v}N_A} \quad (4)$$

$$d_b = \frac{m}{h\pi r^2} \quad (5)$$

$$P = 1 - \frac{\text{db}}{dx} \quad (6)$$

In the aforementioned equations, Avogadro's number is marked as $N_A = 6.0221 \times 10^{23}$, the variable m represents the molar mass of a substance in grams per mole ($g.mol^{-1}$), the atomic number is represented by Z = 8, the unit cell volume is denoted as $V = (a^3)$, the symbol r is used to represent the radius, and the width of a pellet built on nano-composites is indicated by the variable h[26]. The values obtained for both kinds of density are presented in **Table 1**. The density of X-rays (d_x) exhibits a decrease from 5.01–4.91

g.cm^{-3} as the Co^{3+} content increases, specifically for x values of 0.00 and 0.0250. This decrease can be attributed to the direct relationship between mass and density. The bulk density (d_b) exhibits an increase within the range of 3.83–3.84 g.cm^{-3} as a result of Co^{3+} doping. The disparities between d_x and d_b arise from the generation of unoccupied volume during the sintering procedure. **Figure 4** depicts the variations in X-ray density and bulk density with the introduction of Cobalt concentration[27].

The formulas utilized for the calculation of the hopping lengths (L_A and L_B) about the A and B sub-lattice sites, respectively, among magnetic ions are as follows[28]:

$$L_A = a\frac{\sqrt{3}}{4} \tag{7}$$

$$L_B = a\frac{\sqrt{2}}{4} \tag{8}$$

The calculated values for both L_A and L_B are illustrated in **Table 1**. L_A and L_B both decrease with a decrease in lattice constant, grain size as shown in **Figure 5**. This modification may have a significant impact on the magnetic properties and biocompatibility of the material, making it more suitable for biomedical applications[29,30].

Table 1. Results related to XRD peaks of $Zn_{0.5}Ni_{0.5}Fe_{2-x}Co_xO_4$.

Structure parameters	**x = 0.00**	**x = 0.025**
FWHM (radians)	0.002	0.004
2θ (degree)	35.06	35.15
Lattice constant (Å)	8.493	8.470
Volume unit cell (Å)^3	612.79	607.78
Crystallite size(nm)	72.8	18.2
d-spacing	2.561	2.554
Dislocation line density	3.69	14.8
X-rays density (g.cm^{-3})	5.01	4.91
Bulk density (g.cm^{-3})	3.831	3.848
Hopping length, L_A (Å)	3.678	3.668
Hopping length, L_B (Å)	3.01	2.98

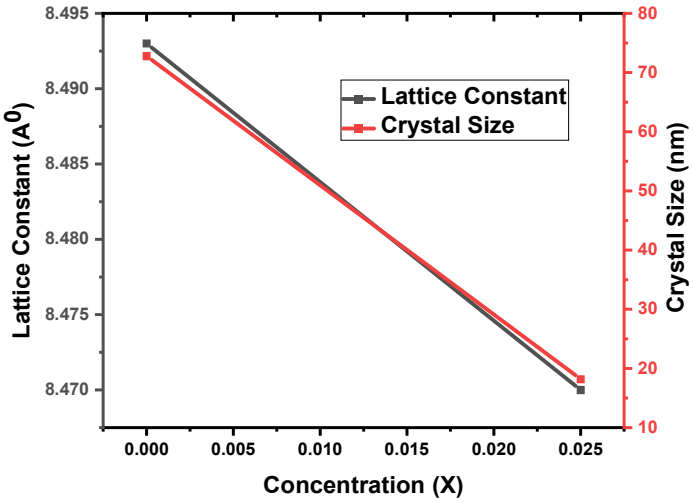

Figure 3. Average crystallite size and lattice constant vs. Co concentration for $Zn_{0.5}Ni_{0.5}Fe_{2-x}Co_xO_4$ for x = 0.00, and 0.0250.

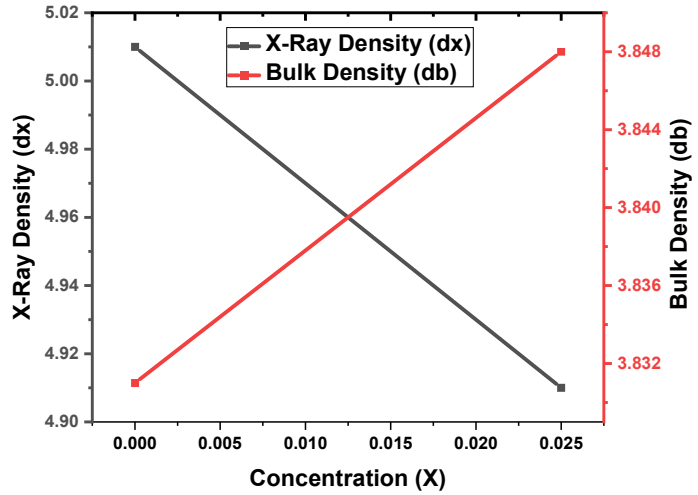

Figure 4. Bulk density and X-Ray density of $Zn_{0.5}Ni_{0.5}Fe_{2-x}Co_xO_4$ for x = 0.00, and 0.0250.

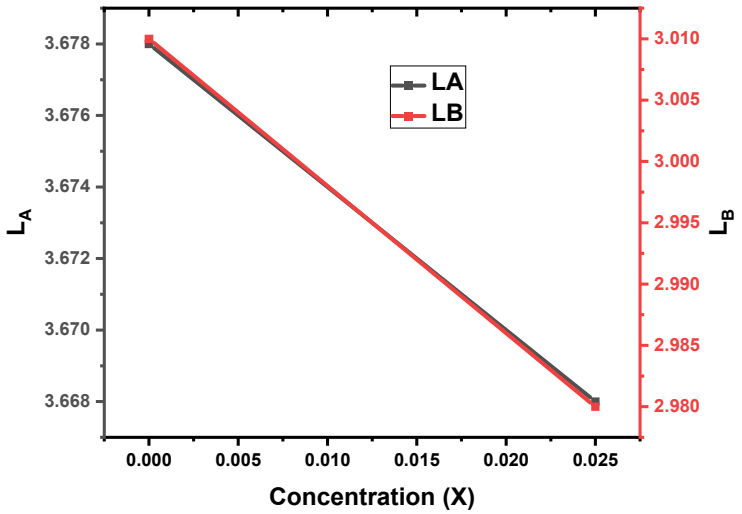

Figure 5. Hopping lengths (LA and LB) against Co concentration.

4. Conclusions

In this study, we have conducted an X-ray Diffraction (XRD) analysis of Co-doped $ZnNiFe_2O_4$ ferrites to assess their structural properties for potential applications in medicine. The XRD results indicate that the doping process has resulted in a modified decrease in lattice parameter (8.493–8.470 Å), grain size (72.8–18.2 nm), and an increase in dislocation line density per meter (3.69–14.8) suggesting the successful incorporation of cobalt into the crystal structure. The Co-doped $ZnNiFe_{2-x}O_4$ spinel ferrite materials become more suitable for medical applications as the decrease in lattice constant, reduction in grain size, and increase in dislocation line density (DLD) enhance their magnetic properties, making them excellent candidates for targeted drug delivery and MRI contrast agents. The decrease in X-ray density (5.01–4.91 g cm^{-3}) and simultaneous increase in bulk density (3.831–3.848 g cm^{-3}) can facilitate better tissue penetration and biocompatibility, making them ideal for non-invasive medical imaging and therapeutic applications, while minimizing potential health risks.

Author contributions

Methodology, AM; visualization, investigation, MIK; data analysis, BA; data curation, software, AK; writing—original draft, AZM; writing—review & editing, AA. All authors have read and agreed to the published version of the manuscript.

Acknowledgments

The authors would like to express their gratitude for the assistance and support received from their institutions and fellow researchers in conducting this study.

Conflict of interest

The authors declare no conflict of interest.

References

1. Rethi NR, Murugeswari A, Sankaranarayanan R. Role of Al^{3+} and Cr^{3+} Ions on structural, optical, magnetic, and impedance properties of $Al_yCr_xZn_{(0.4-y)}Ni_{(0.6-x)}Fe_2O_4$ nanoparticles. *Journal of Superconductivity and Novel Magnetism* 2023; 36: 1443–1454. doi: 10.1007/s10948-023-06579-4
2. Saleem S, Ashiq MN, Manzoor S, et al. Analysis and characterization of opto-electronic properties of iron oxide (Fe_2O_3) with transition metals (Co, Ni) for the use in the photodetector application. *Journal of Materials Research and Technology* 2023; 25: 6150–6166. doi: 10.1016/j.jmrt.2023.07.065
3. Li Y, Shi C, Zhang H, He X, Liu L. Magnetic Properties and Local Structure of the (La, Co) Co-doped Bi1−xLaxFe0.95Co0.05O3. *Crystals* 2021; 11(9): 1059. doi:10.3390/cryst11091059
4. Yu X, Zhou N, Liu R, et al. Effect of Zn^{2+}-Sn^{4+} co-substitution on structural and magnetic properties of $SrFe_{12-2x}Zn_xSn_xO_{19}$ (x = 0–2) M-type strontium ferrite. *Physica B: Condensed Matter* 2023; 653: 414676. doi: 10.1016/j.physb.2023.414676
5. Wan K, Liu W, Ding Y, et al. Comparative investigation of insulation techniques based on APTES for different structures and magnetic properties of soft magnetic composites. *Journal of Magnetism and Magnetic Materials* 2023; 571: 170571. doi: 10.1016/j.jmmm.2023.170571
6. Sheikh FA, Gilani ZA, Noor ul Huda Khan Asghar HM, et al. Structural, morphological, and magneto-dielectric features of Ni-Co-Pr ferrites for high density memory and high frequency devices. *Journal of Magnetism and Magnetic Materials* 2023; 587: 171240. doi: 10.1016/j.jmmm.2023.171240
7. Ameen F, Majrashi N. Recent trends in the use of cobalt ferrite nanoparticles as an antimicrobial agent for disability infections: A review. *Inorganic Chemistry Communications* 2023; 156: 111187. doi: 10.1016/j.inoche.2023.111187
8. Wu X, Ding Z, Song N, et al. Effect of the rare-earth substitution on the structural, magnetic and adsorption properties in cobalt ferrite nanoparticles. *Ceramics International* 2016; 42(3): 4246–4255. doi: 10.1016/j.ceramint.2015.11.100
9. Frei EH, Gunders E, Pajewsky M, et al. Ferrites as contrast material for medical X-ray diagnosis. *Journal of Applied Physics* 1968; 39(2): 999–1001. doi: 10.1063/1.1656366
10. Tamboli QY, Patange SM, Mohanta YK, et al. Green synthesis of cobalt ferrite nanoparticles: An emerging material for environmental and biomedical applications. *Journal of Nanomaterials* 2023; 2023: 9770212. doi: 10.1155/2023/9770212
11. Mujtaba A, Khan MI, Hasan MS, et al. Tailoring the structural, optical, photoluminescence, dielectric and electrical properties of $Zn_{0.6}Ni_{0.2}Mg_{0.2}Fe_{2-x}La_xO_4$ (x= 0.00, 0.0125, 0.0250, 0.0375). *Journal of Materials Research and Technology* 2023; 23: 4538–4550. doi: 10.1016/j.jmrt.2023.02.038
12. Wu Z, Zhang Y, Shan L, Han Z. Properties of Sm–Mn substituted M-type strontium ferrites synthesized by the sol-gel method. *Ferroelectrics* 2023; 614(1): 183–193. doi: 10.1080/00150193.2023.2227081
13. Latif S, Liaqat A, Imran M, et al. Development of zinc ferrite nanoparticles with enhanced photocatalytic performance for remediation of environmentally toxic pharmaceutical waste diclofenac sodium from wastewater. *Environmental Research* 2023; 216(Part 2): 114500. doi: 10.1016/j.envres.2022.114500
14. Hussein MM, Saafan SA, Abosheiasha HF, et al. Crystal structure and peculiarities of microwave parameters of $Co_{1-x}Ni_xFe_2O_4$ nano spinel ferrites. *RSC Advances* 2023; 13(38): 26879–26891. doi: 10.1039/d3ra04557a

15. Katoch G, Himanshi, Jasrotia R, et al. Crystal structure, synthesis, properties and potential applications of cobalt spinel ferrite: A brief review. *Materials Today: Proceedings* 2023; in press.
16. Abdalazeez A, Li T, Liu X, et al. Investigation of $BaFe_2O_4$ oxygen carrier modified by supports in chemical looping gasification of biochar. *International Journal of Hydrogen Energy* 2023; in press.
17. Nguyena NT, Nguyen VA. Ultrasound-assisted sol-gel synthesis, characterization, and photocatalytic application of ZnO nanoparticles. *Digest Journal of Nanomaterials and Biostructures* 2023; 18(3): 889–897. doi: 10.15251/DJNB.2023.183.886
18. Mosleh-Shirazi S, Kasaee SR, Dehghani F, et al. Investigation through the anticancer properties of green synthesized spinel ferrite nanoparticles in present and absent of laser photothermal effect. *Ceramics International* 2023; 49(7): 11293–11301. doi: 10.1016/j.ceramint.2022.11.329
19. Udhaya PA, Ahmad A, Meena M, et al. Copper Ferrite nanoparticles synthesised using a novel green synthesis route: *Structural* development and photocatalytic activity. *Journal of Molecular Structure* 2023; 1277: 134807. doi: 10.1016/j.molstruc.2022.134807
20. Godara SK, Prakash J, Jasrotia R, et al. Green synthesis of magnetic nanoparticles of $BaFe_{12}O_{19}$ hexaferrites using tomato pulp: Structural, morphological, optical, magnetic and dielectric traits. *Journal of Materials* Science*: Materials in Electronics* 2023; 34(20): 1516. doi: 10.1007/s10854-023-10859-z
21. Xing C, Liu CY, Lai C, Zhang SQ. Tuning d-spacing of graphene oxide nanofiltration membrane for effective dye/salt *separation*. *Rare Metals* 2023; 42(2): 418–429. doi: 10.1007/s12598-022-02153-4
22. Thakur A, Verma R, Wan F, et al. Investigation of structural, elastic and magnetic properties of Cu^{2+} ions substituted cobalt nano ferrites. *Journal of Magnetism and Magnetic Materials* 2023; 581: 170980. doi: 10.1016/j.jmmm.2023.170980
23. Arshad M, Khan W, Abushad M, et al. Superior energy storage performance and excellent multiferroic properties in $BaTi_{1-x}Gd_xO_3$ ($0 \leq x \leq 0.06$) ceramics. *Materials Research Bulletin* 2023; 169: 112504. doi: 10.1016/j.materresbull.2023.112504
24. Khan I, Sadiq I, Ashiq MN, Rana MUD. Role of Ce–Mn substitution on structural, electrical and magnetic properties of W-type strontium hexaferrites. *Journal of Alloys and Compounds* 2011; 509(31): 8042–8046. doi: 10.1016/j.jallcom.2011.05.013
25. Vinayak V, Khirade P, Birajdar SD, et al. Low temperature synthesis of magnesium doped cobalt ferrite nanoparticles and their structural properties. *International Advanced Research Journal in Science, Engineering and Technology* 2015; 2(3): 55–58. doi: 10.17148/IARJSET.2015.2313
26. Kale SB, Somvanshi SB, Sarnaik MN, et al. Enhancement in surface area and magnetization of $CoFe_2O_4$ nanoparticles for targeted drug delivery application. *AIP Conference Proceedings* 2018; 1953(1). doi: 10.1063/1.5032528
27. Barkule RS, Kurmude DV, Raut AV, et al. Structural and electrical conductivity studies in nickel ferrite nano-particles. *Solid State Phenomena* 2014; 209: 177–181. doi: 10.4028/www.scientific.net/SSP.209.177
28. Kim DH, Zeng H, Ng TC, Brazel CS. T_1 and T_2 relaxivities of succimer-coated $MFe_2^{3+}O_4$ (M=Mn^{2+}, Fe^{2+} and Co^{2+}) inverse spinel ferrites for potential use as phase-contrast agents in medical MRI. *Journal of Magnetism and Magnetic Materials* 2009; 321(23): 3899–3904. doi: 10.1016/j.jmmm.2009.07.057
29. Amiri M, Salavati-Niasari M, Akbari A. Magnetic nanocarriers: Evolution of spinel ferrites for medical applications. *Advances in Colloid and Interface Science* 2019; 265: 29–44. doi: 10.1016/j.cis.2019.01.003
30. Amiri S, Shokrollahi H. The role of cobalt ferrite magnetic nanoparticles in medical science. *Materials Science and* Engineering*: C* 2013; 33(1): 1–8. doi: 10.1016/j.msec.2012.09.003